THE JOURNAL OF PHYSICAL CHEMISTRY C

Article

Cite This: J. Phys. Chem. C XXXX, XXX, XXX−XXX

pubs.acs.org/JPCC

On the Sputtering of Titanium and Silver onto Liquids, Discussing the Formation of Nanoparticles

Xavier Carette,[†,‡] Benoît Debièvre,[†] David Cornil,[§] Jérôme Cornil,[§] Philippe Leclère,[§] Bjorn Maes,[∥] Nicolas Gautier,[⊥] Eric Gautron,[⊥] Abdel-Aziz El Mel,[⊥] Jean-Marie Raquez,[‡] and Stephanos Konstantinidis*[,†]

[†]Laboratory of Chemistry of Plasma−Surface Interaction (ChIPS), and [‡]Laboratory of Polymeric and Composite Materials (LPCM), University of Mons, 20 Place du Parc, 7000 Mons, Belgium

[§]Laboratory for Chemistry of Novel Materials (CMN), University of Mons, Place du Parc 20, 7000 Mons, Belgium

[∥]Micro- and Nanophotonic Materials Group, Institut de Physique, University of Mons, 20 Place du Parc, 7000 Mons, Belgium

[⊥]Institut des Matériaux Jean Rouxel, Université de Nantes, CNRS, 2 Rue de la Houssinière B.P. 32229, 44322 Nantes Cedex 3, France

Supporting Information

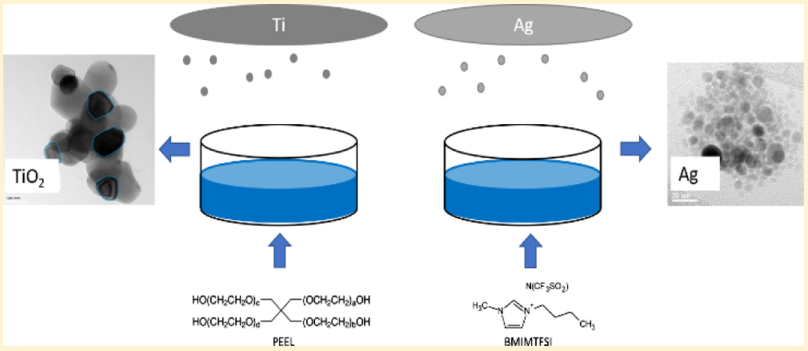

ABSTRACT: Titanium and silver atoms were magnetron-sputtered either onto pentaerythritol ethoxylate (PEEL) or 1-butyl-3-methylimidazolium bis(trifluoromethanesulfonyl)imide (BMIMTFSI) ionic liquid (IL), and the formation of nanoparticles (NPs) is discussed based on the chemical interaction between the metal atoms and the host liquid. In the case of PEEL, our data reveal that titanium atoms sputtered in low-pressure argon plasma first form a film over the liquid surface. However, the latter dissolves as the film gets oxidized when vented to the air; asymmetric and faceted titanium dioxide NPs are finally obtained as if they were originating from a dismantled polycrystalline thin film. In the case of silver sputtered on PEEL, a film forms and solvation never occurs even after exposing the sample to air because the oxidation of silver is thermodynamically much less favorable than titanium. Quantum-chemical calculations confirm that the chemical interaction of TiO_2 with PEEL molecules is favored as compared to metallic Ag or Ti. In contrast to what is observed with PEEL, when silver is sputtered onto the BMIMTFSI IL, no film is observed and spherical and crystallized silver NPs are found. These results suggest that the Ag-NP grows inside the IL because the chemical interaction of the Ag atoms with the BMIMTFSI molecules is highly favorable.

INTRODUCTION

Nanoparticles (NPs) are defined as objects possessing at least one nanometric dimension.[1] NPs have attracted much attention in many fields of research such as catalysis,[2,3] biosensors,[4,5] optoelectronic devices,[5−9] biomedicine,[10−12] or energy conversion.[13−15] This interest is due to the peculiar properties of these nano-objects which originate from the large surface-to-volume ratio and quantum confinement effects.[16] In general, there are two different ways to synthesize nanometric materials, that is, the chemical versus physical strategies.[16] On the one hand, the chemical approach is based on the transformation of single molecules into NPs. Chemical vapor deposition and colloidal synthesis are two chemical processes of this kind. On the other hand, physical methods are based on the transformation of a source material, without modifying its chemical composition, that is, the NPs are formed through the interaction of photons, ions, or heat with matter or by mechanical grinding. Upon ion−surface interactions, a transfer of momentum between fast ions and the topmost atomic layers of a material, that is, the target, allows for the ejection of atoms from the surface. Such ion bombardment is the key feature of the low-pressure (in the Pa range) plasma-based magnetron sputtering technology which has become a standard procedure in the industry for the synthesis of various functional coatings,

Received: July 20, 2018
Revised: October 8, 2018
Published: October 15, 2018

DOI: 10.1021/acs.jpcc.8b06987
J. Phys. Chem. C XXXX, XXX, XXX−XXX

whose thickness typically ranges from few to hundreds of nanometers. The plasma ions, usually argon ions, are accelerated by the negative potential of the cathode which is covered by the metal target to be sputtered. The sputtered particles are transported to the substrate, which, in most of the cases, is a solid such as a glass pane or a steel sheet. On the substrate surface, nucleation and island growth proceed. These phenomena are the basic processes underlying the formation of a continuous coating.

In 1996, Ye and co-workers sputtered silver over a silicon oil.[17] In this case, a silver thin film was produced and no evidence of the presence of silver NPs was reported. A few years later, Wagener et al. reported the production of metallic NPs into the same kind of liquid.[18] Apparently, this oil was not a suitable stabilization agent as NP aggregation and sedimentation appeared. Other articles reported the use of other liquids capable to sustain vacuum processing and to stabilize the NP generated by the sputtering. Ionic liquids (IL),[19−22] organic oils,[23] and vegetable oils[11] are the most used liquids. By sputtering metals onto properly chosen liquids, NPs are generated into a closed reactor and directly incorporated into the liquid medium. The latter situation should guarantee high-purity, transportation safety, and (relatively) well-dispersed NPs inside the liquid.[20] However, according to the review article by Dupont and Scholten,[2] there is still work to be done to understand the growth mechanism of the NPs in such conditions.

In the present article, we discuss two extreme cases of sputtering metal over liquids. First, we sputter titanium and silver onto pentaerythritol ethoxylate (PEEL), an organic oil. Titanium and silver exhibit different physicochemical properties, such as the enthalpy of oxidation. Second, we sputter silver onto the IL, 1-butyl-3-methylimidazolium bis-(trifluoromethanesulfonyl)imide (BMIMTFSI), which obviously exhibits different properties compared to PEEL. Through this study, we discuss how the nature of the sputtered metal and liquid substrate plays a role on: (i) the NP growth mechanisms and (ii) the morphology of the resulting NPs.

MATERIALS AND METHODS

The BMIMTFSI IL with a purity of 99% was purchased from Solvionic. The bottle containing the IL was opened and kept in a glovebox to avoid any contamination of atmospheric water which could lead to the sedimentation of the particles.[20] The ILs are organic salts which possess a melting temperature below 100 °C. These ILs have an extremely low vapor pressure which allows them to be used under vacuum, that is, in a plasma chamber. BMIMTFSI was chosen because of its transparency in the UV−vis range. The second liquid, PEEL, was purchased from Sigma-Aldrich, and no special care was taken regarding stocking.

The schematic view of the vacuum chamber utilized for the sample preparation is presented on Figure 1. For the sputtering experiments, 4 mL of liquid was poured into a cylindrical ceramic crucible (4.5 cm in diameter, 4 cm in height) located at 15 cm from the magnetron cathode surface which was holding the target to be sputtered (see Figure 1). The cathode is furnished with a pair of permanent magnets that allow trapping the plasma near the sputtering target surface. For the present experiments, we used either a 5.1 cm in diameter Ti target or a 7.5 cm in diameter silver target. The electrical power applied to the cathode was 20 W in both cases. The power density was then ∼0.4 W/cm^2 for the Ti target and ∼1

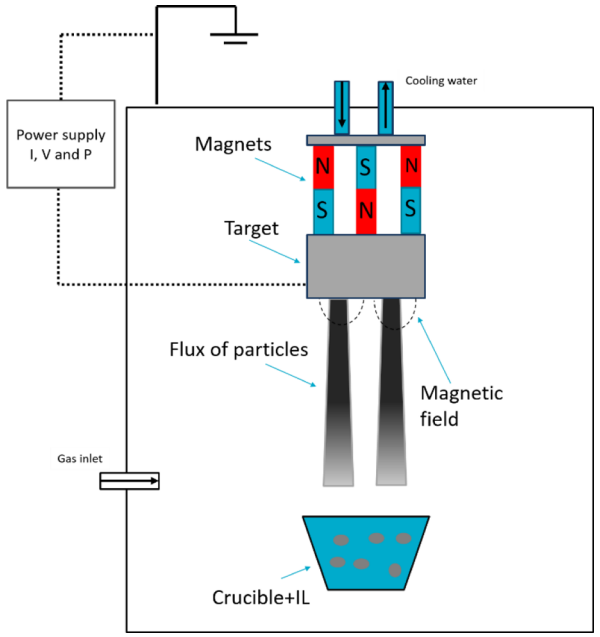

Figure 1. Schematic representation of the deposition setup.

W/cm^2 for the Ag target. The purity of these materials was 99.99% for silver and 99.7% for titanium. The pressure (argon) was kept constant during the sputtering process. For titanium, the presented data were obtained for a total pressure of 5 mTorr (0.7 Pa). For silver sputtering experiments, the pressure was kept to 10 mTorr (1.3 Pa).

After placing the liquid inside the vacuum chamber for deposition, the chamber was pumped down in two steps. First, the primary pump (EDWARDS RV3) was turned on to achieve a residual pressure of 10^{-2} Torr (∼10 Pa). Finally, the turbomolecular pump (PFEIFFER D35614) allowed reaching 10^{-7} Torr (∼10^{-5} Pa). The high-purity argon gas was then injected in the system. The flow is typically in the range of a few standard cubic centimeter per minute (sccm) and is controlled via a digital mass flow controller. In this way, the composition of the working atmosphere and the plasma chemistry is controlled. To reach the setpoint pressure, a throttle valve, set in front of the turbomolecular pump, regulates the pumping speed. It should be noted that prior to any sputtering experiment, the target surface was sputter-cleaned in argon plasma. A removable steel shutter (not shown on Figure 1) was moved in front of the sputter target to avoid depositing materials on the liquid substrate located below during the cleaning process. Once the surface chemistry is stabilized, as verified by monitoring the target current and voltage displayed by the electric power supply (Advanced Energy MDX 500), the plasma was turned off and the protecting shutter set aside. The plasma was then reignited again to perform the deposition onto the liquid substrate, with a defined target chemistry. The deposition rate, that is, the mass of deposited material per unit time, was obtained for each plasma condition by weighting a ∼2 × 2 cm^2 silicon wafer substrate onto which the material was sputtered for a given duration. Hence, the liquid solution could be loaded with a known amount of sputtered material. Using the above-mentioned deposition conditions, the deposition rate was 2.5 μg/min (5 × 10^{-8} mol/min) in the case of titanium sputtering and 215 μg/min (2 × 10^{-6} mol/min) in the case of silver deposition. After deposition, the samples were kept in a

DOI: 10.1021/acs.jpcc.8b06987
J. Phys. Chem. C XXXX, XXX, XXX−XXX

glovebox in the case of the IL solutions. No particular care was taken for the stocking of the PEEL samples.

To get further insights into the chemical interactions between the PEEL organic oil and the different NPs, quantum-chemical calculations were carried out at the density functional theory (DFT) level with periodic boundary conditions used to model a flat substrate, as implemented in the SIESTA 4.0 code.[24] The exchange−correlation functional is described within the general gradient approximation using the Perdew−Burke−Ersenoff functional.[25] A double-ζ polarized numerical atomic basis set is adopted for the valence electrons with a mesh cutoff of 250 Ry for the real-space grid, whereas core electrons are described with Troullier−Martin pseudopotentials.[26] A Monkhorst−Pack grid of $(2 \times 2 \times 1)$ was used during the relaxation of the interface and increased to $(4 \times 4 \times 1)$ for the calculation of the adsorption energy. For the sake of computational facility, a simplified version of the PEEL organic oil was used by shortening the aliphatic chain to end up with a pentaerythriol molecule $C(CH_2OH)_4$. This molecule is first fully relaxed in the isolated state using a large unit cell of $(30 \times 30 \times 30)$ Å^3 to avoid intermolecular interactions. We then characterized the interaction of this model molecule with several surfaces, representing the metal-based NP, made of pure and oxidized titanium and silver by considering the stable crystalline Ti(0001), TiO_2(101), Ag(111), Ag_2O(111), and AgO(111) surfaces. The details about the model surfaces are provided in the Supporting Information.

The interaction of pentaerythritol with each surface was modeled by approaching the neutral molecule close to the surface with one or two functional groups oriented toward the surface to favor either a monodentate or bidentate configuration. Chemisorption or physisorption was assessed by the adsorption energies. The geometric relaxation was performed using the conjugate gradient formalism with a convergence criterion on the atomic forces of 0.04 eV Å^{-1}. The molecule and the top two layers were allowed to relax, whereas the three bottom layers were frozen in their bulk geometry. The interaction energy was calculated on the final relaxed geometry using the expression

$$E_{int} = E_{surf/mol} - [E_{mol} + E_{surf}]$$

where $E_{surf/mol}$ is the energy of the full system in its optimized geometry and E_{mol} and E_{surf} are the energy of the isolated neutral molecule and the surface in the interface geometry, respectively.

The solutions loaded with NP were poured in a quartz cell (Hellma 100-QX) and analyzed by UV−visible spectroscopy using a PerkinElmer LAMBDA 650S device. For the IL solutions, the cells were filled and closed in a glovebox. The morphology of the particles was monitored using a Hitachi H9000-NAR transmission electron microscope (TEM) with an acceleration voltage of 300 kV. The samples made of PEEL were prepared for TEM analysis by pouring a drop of the NP-containing solution onto a TEM Cu grid coated with a holey carbon foil. The latter was put in ethanol to remove the excess of oil from the sample. For the IL solutions, a different method was used. The samples were centrifuged with a small amount of acetone for 30 min followed by three cycles in ethanol to isolate the particles. The particles were then drop-cast onto a TEM grid (Cu with a holey carbon foil). Some samples were also analyzed by atomic force microscopy (AFM) in the Tapping mode using a Dimension Icon equipped with a Nanoscope V controller from Bruker (Santa Barbara, CA) at room temperature in air, using microfabricated cantilevers (spring constant of 30 N/m and a resonance frequency about 300 kHz). The images were recorded with the maximum available number of pixels (512) in each direction and are shown as captured.

Finally, in the case of silver NP solutions, simulated spectra were obtained with the Mieplot software[27] assuming spherical silver particles in the IL medium. The IL liquid was not present in the database of Mieplot software. To simulate it, we used the refractive index value (n = 1.3895) provided in ref 28.

RESULTS AND DISCUSSION

Titanium was sputtered over the PEEL solution, using argon plasma. The sputter power was 20 W, and the argon pressure was set to 5 mTorr (0.7 Pa). The presence of a film on the surface of the liquid was observed when the sample was taken out of the vacuum chamber. This film even remained on the surface of the liquid when stored during several days in the chamber, in an argon atmosphere (5 mTorr). However, the film broke down as the vacuum chamber was vented (and the film allowed to interact with air) and film debris precipitated at the bottom of the flask. After a few days, the film solid residues could not be distinguished by naked eye.

If the chemical interaction between the sputtered titanium atoms and the PEEL oil is not favorable, one may expect the solvation of the sputtered metal atoms to be prevented, or at least, the solvation process to be very slow and the sputtered metal atoms impinging on the surface of the PEEL solution to behave as if they were landing onto a solid surface. Namely, sputtered metal atoms reach the liquid surface onto which they diffuse, nucleate, and form islands which may grow laterally and in height to finally form an apparently continuous film, as schematically represented in Figure 1 in ref 29. On the other hand, because of the very good affinity of Ti for O and the thermodynamically favorable formation of Ti−O bonds (bond formation enthalpy of −305.43 kJ/mol[30]), the film gets oxidized in contact with air during the venting process. At this moment, the affinity between the PEEL molecules and the surface of the newly oxidized metal is enhanced and solvation of the multitude of islands forming the film may eventually start.

From the results presented in Table 1, it appears that for titanium, the bidentate binding of the PEEL molecule is more favorable because the calculated adsorption energy is almost twice larger (0.64 eV vs 0.39 eV) compared to the

Table 1. Calculated Interaction Energies between the (OH-Terminated) Model PEEL Oil Molecules and Different Surfaces

nature of the surface	binding mode	adsorption energy (eV)
Ag	monodentate	−0.15
	bidentate	−0.10
Ag_2O	monodentate	−0.96
	bidentate	−1.54
AgO	monodentate	−0.28
	bidentate	−1.13
TiO_2	monodentate	−1.12
	bidentate	−2.32
Ti	monodentate	−0.39
	bidentate	−0.64

DOI: 10.1021/acs.jpcc.8b06987
J. Phys. Chem. C XXXX, XXX, XXX−XXX

monodentate binding scheme because of the formation of two new covalent bonds instead of one. Furthermore, the binding energy is significantly enlarged for the TiO_2 surface, that is, −1.12 and −2.32 eV for the monodentate and bidentate modes, respectively. This result supports the concept of oxidation-enabled solvation of the sputtered material in the case of the PEEL solutions. Finally, the calculations highlight that silver does not interact favorably with the organic oil because the binding energy is rather small (0.10−0.15 eV, see Table 1). However, the interaction of Ag_2O and AgO with the PEEL molecules is more energetically favorable. Similarly, it is found for silver oxide surfaces that the interaction is reinforced when considering bidentate binding modes. The different structures are shown in the Supporting Information

Figure 2 presents the UV−vis absorption spectrum of a PEEL solution after the film has dissolved. A shoulder appears

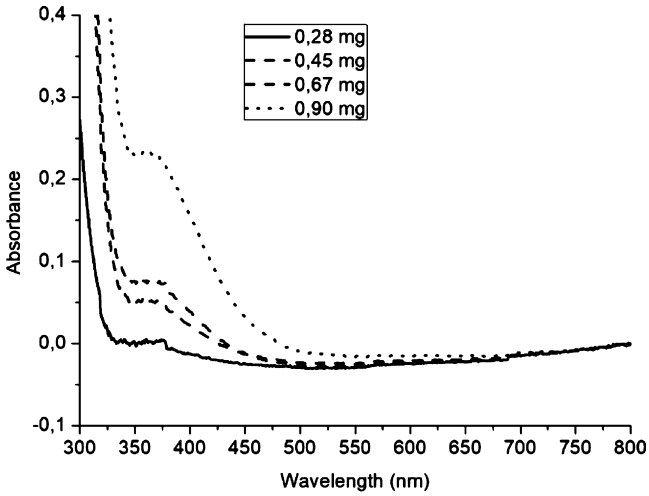

Figure 2. UV−visible absorption spectrum for plasma-treated oil at 20 W, 5 mTorr and loaded with various contents of titanium.

in the UV−vis spectrum around 350−370 nm. The shoulder is more pronounced as the amount of sputtered metal increases, that is, the treatment time is increased, and more material is deposited onto the liquid surface. Bulk TiO_2 is characterized by a band gap energy of typically ∼3.2 eV which induces light absorption around 390 nm.[28] Hence, the apparition of a shoulder on the absorption spectrum after plasma sputtering of the Ti atoms could be attributed to the presence of NPs made of TiO_2 as observed in refs 31 and 32.

From Figure 3, one can note on the TEM micrographs that the NPs are indeed detected and present an anisotropic and faceted shape, which are expected if the NP formation takes place at the surface of the PEEL oil. Indeed, such faceted crystals were observed by TEM when atoms are sputtered onto a solid surface, see for example, Figure 2 in the works of Barna and Adamik[33] and Figure 2 in ref 29. In the present working conditions, if the oil indeed behaves as a solid surface because no solvation can occur, film formation may proceed from nucleation to island formation toward, at the end, the production of a (quasi) continuous film where islands are connected by grain boundaries.[29]

TEM evidences that NPs are well faceted (Figure 3) and selected-area electron diffraction (SAED) highlights that the NPs extracted from the PEEL oil are made of TiO_2 and are crystallized into the anatase phase (Figure 4). The morphology

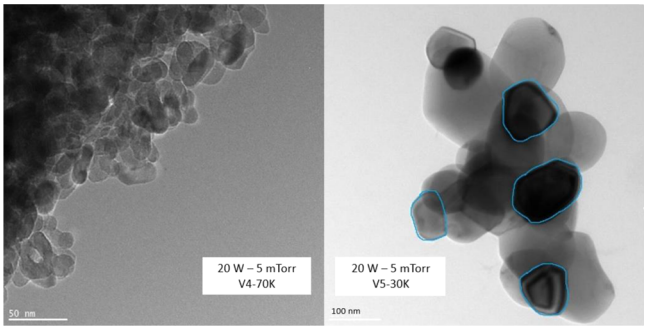

Figure 3. TEM pictures of the NPs found inside the PEEL solutions. Deposition power and pressure were 20 W and 5 mTorr, respectively. Sputtering was carried out in argon. Blue lines are added to distinguish some of the particles.

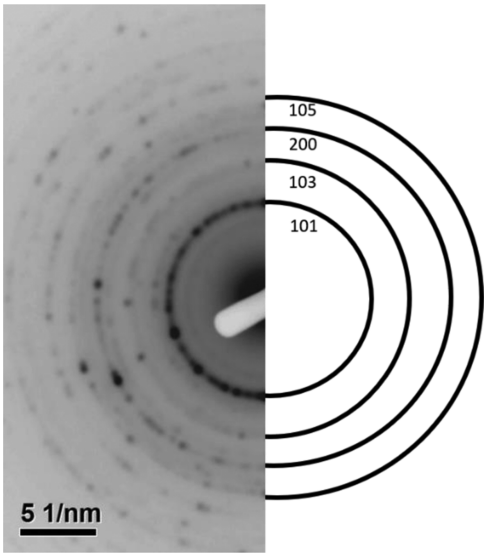

Figure 4. Experimental electron diffraction pattern of an agglomeration of TiO_2 particles (left side). The rings can be indexed with anatase TiO_2 structure (right side).

and size of the NP obtained when titanium was sputtered in argon were analyzed. As presented on Figure 3, the NPs are agglomerated and have variable sizes, ranging from ∼30 to ∼150 nm. This agglomeration could be explained by three phenomena. First, it can be attributed to the TEM sample preparation procedure. Second, this agglomeration can arise from the fact that a film forms on the surface of the oil. In that case, the affinity of the oil for titanium is not sufficient to provoke a complete degradation of the film into well-dispersed NPs in the absence of oxygen during the sputtering process and some islands are still connected to one another and, third, the PEEL molecules do not fully stabilize the NPs.

Because no sedimentation was observed for the various samples of TiO_2 produced into PEEL, a stabilizing shell should protect the NPs. Actually, this shell can be observed through AFM analysis. Few drops of the NP-containing PEEL solution were transferred onto a glass plate and then washed with diethyl ether to remove the excess of PEEL. On Figure 5, corresponding to the topographic image, the dark spot in the center of each bright disk corresponds to NPs. The large disk is made of liquid which provokes the typical wavy unstable signal during AFM imaging. This observation highlights the rather strong interaction between the PEEL molecules and the

DOI: 10.1021/acs.jpcc.8b06987
J. Phys. Chem. C XXXX, XXX, XXX−XXX

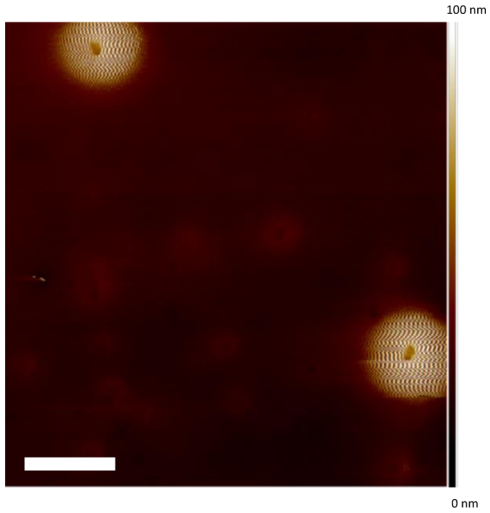

Figure 5. AFM pictures of isolated NPs on a glass substrate (scale bar = 1 μm).

surface of the NP, as highlighted for a TiO_2 surface and the −OH-terminated PEEL molecules by the DFT calculations (Table 1). The rings have a diameter of several hundreds of nanometers, whereas the NPs have a diameter of several tens of nanometers. The observation of such large liquid shells can be here attributed to a spreading effect because of the physicochemical interactions between the PEEL molecules and the surface of the glass slide. This situation would promote a steric hindrance stabilization mechanism for the TiO_2-NP inside the PEEL liquid. Also, it should be noted that in our working conditions, no precipitates inside the PEEL liquid could be observed by the naked eye after the solubilization of the film and the solution remained transparent.

As discussed above, enabling a proper liquid−metal surface interaction is key for the solvation of the sputtered particles and the formation of NPs. In this second experiment, silver atoms were sputtered using the same deposition apparatus. In this case, the sputter power was 20 W and the working pressure equal to 10 mTorr (1.3 Pa). The sputtering process resulted in the production of a film at the surface of the oil (Figure 6a). Contrarily to the case of titanium discussed above

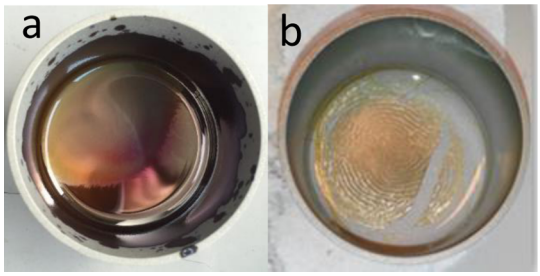

Figure 6. Visual aspects of the (a) silver on PEEL and (b) Ti on PEEL.

(Figure 6b), the silver film never solubilized after venting the chamber and getting exposed to air. Large agglomerates, visible with the naked eye, are precipitating in the bottom of the vial.

Although the theoretical data highlight the rather favorable interaction of the PEEL molecules with the oxidized silver surfaces, according to the enthalpy of oxidation, the oxidation of silver (ΔH = −30.6 kJ/mol) is much less likely to happen upon venting the sample, as compared to titanium (ΔH = −305.43 kJ/mol). Silver thus stays mainly metallic and is not dispersed inside the PEEL solution.

Finally, silver was sputtered over the BMIMTFSI IL. According to ref 16 and references presented therein, IL allows for the production of metal NPs through sputtering. In our case and for the sake of comparison, the Ag sputtering experiments were carried out with a 2 in. silver target, using the same apparatus (sputter power of 20 W, and a 10 mTorr argon pressure) as for sputter deposition onto PEEL.

In the case of BMIMTFSI and contrarily to the previous sputtering experiments of Ag onto PEEL, no film formation on the surface of the IL was ever observed when venting the sample. On the other hand, one could observe with the naked eye a cloud of particles located underneath the surface of the liquid. This behavior is similar to what Tsuda et al. reported.[34] These observations emphasize that the interaction between the IL surface and the sputtered metal atoms is different as compared to the situation encountered with the PEEL solution. The presence of such a high-concentration region under the surface can be explained by the fact that metal−IL molecule is rather efficient to promote a relatively rapid incorporation of the silver atoms into the liquid and that their diffusion is slow due to the rather high viscosity of the IL (viscosity = 61.14 cP). The nucleation and growth of the NPs would therefore mostly occur inside the solution. The interaction of the Ag-NP with BMIMTFSI molecules is most likely of electrosteric nature, as reported in ref 22. However, in their recent review, Wegner and Janiak[35] state: "the interaction between an IL and a (growing) metal NP is far from understood. Factors such as IL-viscosity, hydrogen-bonding capability, and the relative ratio of polar and nonpolar domains of ILs may also influence the stability of NPs in ILs and an improved understanding of the IL−NP interaction would be needed for a more rational design of nanomaterials in ILs".

These IL−Ag solutions were analyzed, and UV−vis absorption spectra were recorded. An absorption peak appears at 410 nm, as reported on Figure 7. Spectra were recorded as a function of time. Figure 7 shows the evolution of the absorption spectrum, starting almost immediately after venting the sample and introducing it in the spectrophotometer (0 min curve) up to a waiting time equal to 24 h. From these data, one can extract two pieces of information. A characteristic absorption peak (around 400 nm) of the electromagnetic spectrum is observed, that is, the IL solution has turned to yellow. This proves the presence of silver NPs. Second, the solution of NP is not fully stable over time because the plasmonic peak intensity decreases with time. When the peak intensity diminishes, another peak is found to increase in intensity at ∼600 nm. This second peak appears a few minutes after the first scan and shifts to higher wavelength with time. This second peak is best observed on the curve corresponding to a waiting time of 24 h. This kind of behavior has already been reported in the literature[20,36] and can be attributed to NPs agglomerating inside the solution because of the presence of water inside the IL solution. Indeed, during the experiment, the IL is in contact with air when inserting and pulling out the sample in the plasma reactor. The vial used for the UV−vis measurements was not gas tight either. This could allow the IL solution to interact with ambient water vapor.

One can use the UV−vis spectra and the Mie theory to calculate the approximate diameter of the particles. Simulated spectra were obtained with the Mieplot software.[27] In our case,

DOI: 10.1021/acs.jpcc.8b06987
J. Phys. Chem. C XXXX, XXX, XXX−XXX

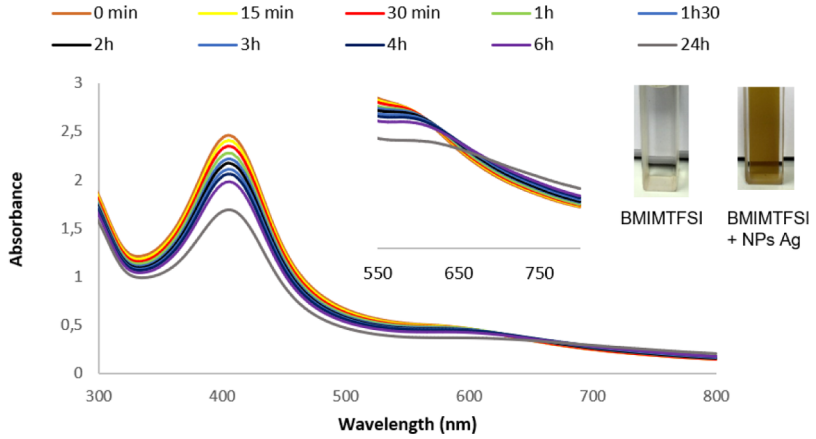

Figure 7. UV−visible spectra of the Ag−IL solution. Deposition power and pressure were 20 W and 10 mTorr. Sputtering was carried out in argon (0.539 mg of silver in 4 mL of IL).

the best fit between the theoretical and experimental spectra was obtained for an average diameter of 15 nm. It should be noted here that this theoretical fit does not take account of the width of the plasmon peak. The width of this peak is an important factor related to the dispersion in size.

According to TEM pictures (Figure 8), one can find that the NPs are indeed spherical and have a diameter ranging from ∼5 up to ∼20 nm, in line with the average value obtained through simulation by the Mie theory of the UV−vis absorption data. The statistical size dispersion cannot be readily calculated from the TEM pictures because of the agglomeration of the particles. Because of the spherical shape of those NPs, one could expect that they are not formed on the surface of the liquid, as in the case of sputtering titanium on PEEL solutions, but rather inside the (homogeneous) liquid medium. This situation corresponds to the growth mechanism II presented on Figure 9 for atoms sputtered onto IL solution in the review article of Wender et al.[16]

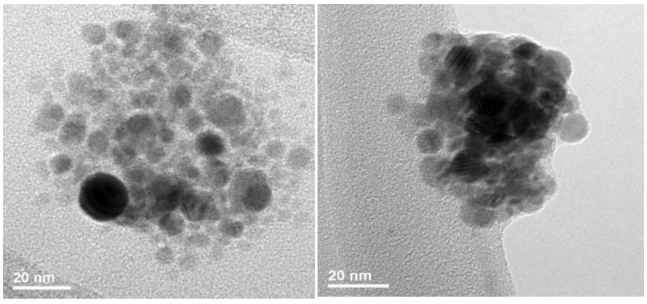

Figure 8. TEM pictures of silver NPs as produced when sputtering silver onto BMIM TFSI IL (power = 20 W, pressure = 10 mTorr).

The TEM SAED analysis carried out on those samples is presented on Figure 8. The experimental diffraction patterns highlight the presence of crystallized silver NPs.

From the results obtained on BMIMTFSI IL, one can conclude that the interaction between the sputtered materials is different as compared to what is obtained with the PEEL solution when sputtering titanium or silver. The modification in the metal−liquid surface combination leads to a change in the growth mechanism of the NPs which, ultimately, induces the formation of spherical NPs.

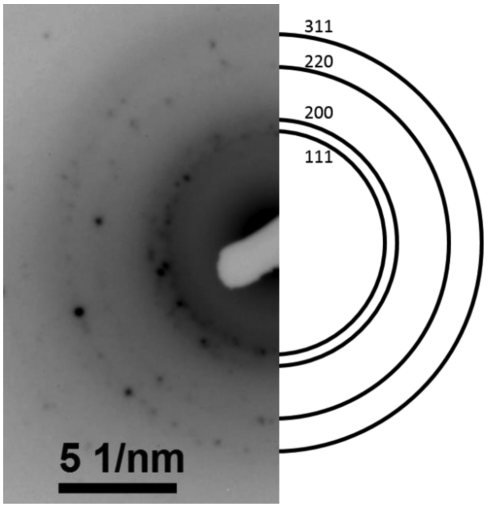

Figure 9. Experimental electron diffraction pattern of an agglomeration of silver particles (left side). The rings can be indexed with a fcc Ag structure (right side).

CONCLUSIONS

Titanium and silver metal targets were sputtered over liquid substrates using a low-pressure magnetron plasma. The working atmosphere was pure argon to allow for the generation of a vapor of metal atoms. Two liquids were utilized: PEEL and BMIMTFSI having different interactions with the sputtered metal atoms. Varying the deposition conditions allowed us to shed some light on the requirements for promoting the growth of NPs in such conditions.

As schematized on Figure 10 (left-hand side column), in the case of PEEL, an OH-functionalized molecule, it is necessary for titanium to be oxidized to enable a proper solvation of the sputtered material. When the pure metal is deposited, a film forms on the PEEL surface because of the low affinity of the PEEL molecule for metallic titanium. If the film gets oxidized, solvation of the numerous nanoislands composing the "continuous" film is enabled, as supported by DFT calculations. In this situation, platelet-like faceted NPs of TiO_2 are obtained. The appearance of those NPs matches well with the island growth mode reported in numerous studies dealing with the sputtering of material over (solid) surfaces. In the case of silver sputtered as a metal, a film forms as well although the latter cannot be solvated by the PEEL molecules

DOI: 10.1021/acs.jpcc.8b06987
J. Phys. Chem. C XXXX, XXX, XXX−XXX

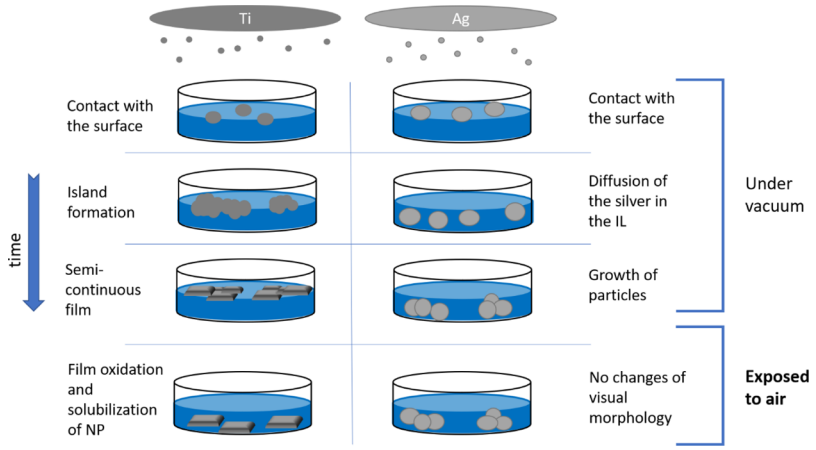

Figure 10. Schematic mechanism for sputtering of titanium onto PEEL (left-hand side) and silver into BMIMTFSI (right-hand side).

upon venting the sample because the affinity of silver for oxygen is much smaller than for titanium. Oxidation of silver does not occur and, ultimately, the silver film precipitates in the PEEL solution.

When sputtering silver atoms onto the IL liquid, a different behavior was observed. This situation is schematically represented on Figure 10 (right-hand side column). Spherical and crystallized silver NPs were obtained which may be explained by the favorable interaction between the IL molecules and the silver atoms. This situation enables the growth of silver NP inside the homogeneous IL solution.

■ ASSOCIATED CONTENT

Supporting Information

The Supporting Information is available free of charge on the ACS Publications website at DOI: 10.1021/acs.jpcc.8b06987.

Generation of the model surfaces and the relaxed interface geometries of the DFT calculations (PDF)

■ AUTHOR INFORMATION

Corresponding Author

*E-mail: stephanos.konstantinidis@umons.ac.be.

ORCID

Xavier Carette: 0000-0002-1317-3264
David Cornil: 0000-0002-9553-1626
Jérôme Cornil: 0000-0002-5479-4227
Abdel-Aziz El Mel: 0000-0003-0923-1043
Jean-Marie Raquez: 0000-0003-1940-7129
Stephanos Konstantinidis: 0000-0002-1672-309X

Notes

The authors declare no competing financial interest.

■ ACKNOWLEDGMENTS

S.K. is Research Associate, P.L. is Senior Research Associate, and J.C. is Research Director of the National Fund for Scientific Research (FNRS), Belgium.

■ REFERENCES

(1) Schmid, G. *Nanoparticles*; Wiley-VCH Verlag GmbH & Co. KGaA: Weinheim, 2005.

(2) Dupont, J.; Scholten, J. D. On the Structural and Surface Properties of Transition-Metal Nanoparticles in Ionic Liquids. *Chem. Soc. Rev.* **2010**, *39*, 1780−1804.

(3) Wang, Y.; Matyjaszewski, K. ATRP of MMA in Polar Solvents Catalyzed by $FeBr_2$ without Additional Ligand. *Macromolecules* **2010**, *43*, 4003−4005.

(4) Yan, Y.; Zhang, Y.; Zeng, H.; Zhang, J.; Cao, X.; Zhang, L. Tunable Synthesis of In_2O_3 Nanowires, Nanoarrows and Nanorods. *Nanotechnology* **2007**, *18*, 175601.

(5) Ramesh, G. V.; Radhakrishnan, T. P. A Universal Sensor for Mercury (Hg, Hg I, Hg II) Based on Silver Nanoparticle-Embedded Polymer Thin Film. *ACS Appl. Mater. Interfaces* **2011**, *3*, 988−994.

(6) Corrêa, N. F.; Santos, C. E. A.; Valadão, D. R. B.; de Oliveira, L. F.; Dupont, J.; Alencar, M. A. R. C.; Hickmann, J. M. Third-Order Nonlinear Optical Responses of Colloidal Ag Nanoparticles Dispersed in $BMIBF_4$ Ionic Liquid. *Opt. Mater. Express* **2016**, *6*, 244.

(7) Li, J.; Zhang, J. Z. Optical Properties and Applications of Hybrid Semiconductor Nanomaterials. *Coord. Chem. Rev.* **2009**, *253*, 3015−3041.

(8) Barnes, W. L.; Dereux, A.; Ebbesen, T. W. Surface plasmon subwavelength optics. *Nature* **2003**, *424*, 824−830.

(9) Chen, H.-T.; Lin, H.-L.; Chen, I.-G.; Kuo, C. Conducting Silver Networks Based on Electrospun Poly(Methyl Methacrylate) and Silver Trifluoroacetate. *ACS Appl. Mater. Interfaces* **2015**, *7*, 9479−9485.

(10) Gao, X.; Cui, Y.; Levenson, R. M.; Chung, L. W. K.; Nie, S. In vivo cancer targeting and imaging with semiconductor quantum dots. *Nat. Biotechnol.* **2004**, *22*, 969−976.

(11) Wender, H.; de Oliveira, L. F.; Feil, A. F.; Lissner, E.; Migowski, P.; Meneghetti, M. R.; Teixeira, S. R.; Dupont, J. Synthesis of Gold Nanoparticles in a Biocompatible Fluid from Sputtering Deposition onto Castor Oil. *Chem. Commun.* **2010**, *46*, 7019−7021.

(12) Rosi, N. L.; Mirkin, C. A. Nanostructures in Biodiagnostics. *Chem. Rev.* **2005**, *105*, 1547−1562.

(13) Kongkanand, A.; Tvrdy, K.; Takechi, K.; Kuno, M.; Kamat, P. V. Quantum Dot Solar Cells. Tuning Photoresponse through Size and Shape Control of CdSe - TiO_2 Architecture. *J. Am. Chem. Soc.* **2008**, *130*, 4007−4015.

(14) Wang, H.; Liu, Y.; Li, M.; Huang, H.; Xu, H. M.; Hong, R. J.; Shen, H. Multifunctional TiO_2 Nanowires-Modified Nanoparticles Bilayer Film for 3D Dye-Sensitized Solar Cells. *Optoelectron. Adv. Mater., Rapid Commun.* **2010**, *4*, 1166−1169, DOI: 10.1039/C4FD00208C.

(15) Chen, X.; Jia, B.; Saha, J. K.; Cai, B.; Stokes, N.; Qiao, Q.; Wang, Y.; Shi, Z.; Gu, M. Broadband Enhancement in Thin-Film Amorphous Silicon Solar Cells Enabled by Nucleated Silver Nanoparticles. *Nano Lett.* **2012**, *12*, 2187−2192.

(16) Wender, H.; Migowski, P.; Feil, A. F.; Teixeira, S. R.; Dupont, J. Sputtering Deposition of Nanoparticles onto Liquid Substrates: Recent Advances and Future Trends. *Coord. Chem. Rev.* **2013**, *257*, 2468−2483.

DOI: 10.1021/acs.jpcc.8b06987
J. Phys. Chem. C XXXX, XXX, XXX−XXX

(17) Ye, G.-x.; Zhang, Q.-r.; Feng, C.-m.; Ge, H.-l.; Jiao, Z.-k. Structural and Electrical Properties of a Metallic Rough-Thin-Film System Deposited on Liquid Substrates. *Phys. Rev. B: Condens. Matter Mater. Phys.* **1996**, *54*, 14754−14757.
(18) Wagener, M.; Günther, B. Sputtering on Liquids - A Versatile Process for the Production of Magnetic Suspensions? *J. Magn. Magn. Mater.* **1999**, *201*, 41−44.
(19) Suzuki, T.; Okazaki, K.-i.; Suzuki, S.; Shibayama, T.; Kuwabata, S.; Torimoto, T. Nanosize-Controlled Syntheses of Indium Metal Particles and Hollow Indium Oxide Particles via the Sputter Deposition Technique in Ionic Liquids. *Chem. Mater.* **2010**, *22*, 5209−5215.
(20) Vanecht, E.; Binnemans, K.; Seo, J. W.; Stappers, L.; Fransaer, J. Growth of Sputter-Deposited Gold Nanoparticles in Ionic Liquids. *Phys. Chem. Chem. Phys.* **2011**, *13*, 13565−13571.
(21) Okazaki, K.-i.; Kiyama, T.; Hirahara, K.; Tanaka, N.; Kuwabata, S.; Torimoto, T. Single-Step Synthesis of Gold-Silver Alloy Nanoparticles in Ionic Liquids by a Sputter Deposition Technique. *Chem. Commun.* **2008**, 691−693.
(22) He, Z.; Alexandridis, P. Nanoparticles in Ionic Liquids: Interactions and Organization. *Phys. Chem. Chem. Phys.* **2015**, *17*, 18238−18261.
(23) Nakagawa, K.; Narushima, T.; Udagawa, S.; Yonezawa, T. Preparation of Copper Nanoparticles in Liquid by Matrix Sputtering Process. *J. Phys.: Conf. Ser.* **2013**, *417*, 012038.
(24) Artacho, E.; Anglada, E.; Diéguez, O.; Gale, J. D.; García, A.; Junquera, J.; Martin, R. M.; Ordejón, P.; Pruneda, J. M.; Sánchez-Portal, D.; et al. The SIESTA Method; Developments and Applicability. *J. Phys.: Condens. Matter* **2008**, *20*, 064208.
(25) Perdew, J. P.; Burke, K.; Wang, Y. Generalized Gradient Approximation for the Exchange-Correlation Hole of a Many-Electron System. *Phys. Rev. B: Condens. Matter Mater. Phys.* **1996**, *54*, 16533−16539.
(26) Troullier, N.; Martins, J. L. Efficient Pseudopotentials for Plane-Wave Calculations. II. Operators for Fast Iterative Diagonalization. *Phys. Rev. B: Condens. Matter Mater. Phys.* **1991**, *43*, 8861−8869.
(27) Laven, P. MiePlot, A computer program for scattering of light from a sphere using Mie theory & the Debye series. http://www.philiplaven.com/mieplot.htm (accessed Sept 7, 2016).
(28) Seki, S.; Tsuzuki, S.; Hayamizu, K.; Umebayashi, Y.; Serizawa, N.; Takei, K.; Miyashiro, H. Comprehensive Refractive Index Property for Room-Temperature Ionic Liquids. *J. Chem. Eng. Data* **2012**, *57*, 2211−2216.
(29) Petrov, I.; Barna, P. B.; Hultman, L.; Greene, J. E. Microstructural Evolution during Film Growth. *J. Vac. Sci. Technol., A* **2003**, *21*, S117−S128.
(30) Chase, M. W.; Curnutt, J. L.; Hu, A. T.; Prophet, H. JANAF Thermochemical Tables, 1974 Supplement. *J. Phys. Chem. Ref. Data* **1974**, *3*, 311−480.
(31) Reddy, K. M.; Reddy, C. V. G.; Manorama, S. V. Preparation, Characterization, and Spectral Studies on Nanocrystalline Anatase TiO2. *J. Solid State Chem.* **2001**, *158*, 180−186.
(32) Valencia, S.; Marin, J. M.; Restrepo, G. Study of the Bandgap of Synthesized Titanium Dioxide Nanoparticules Using the Sol-Gel Method and a Hydrothermal Treatment. *Open Mater. Sci. J.* **2010**, *4*, 9−14.
(33) Barna, P. B.; Adamik, M. Fundamental Structure Forming Phenomena of Polycrystalline Films and the Structure Zone Models. *Thin Solid Films* **1998**, *317*, 27−33.
(34) Tsuda, T.; Imanishi, A.; Torimoto, T.; Kuwabat, S. Nanoparticle Preparation in Room-Temperature Ionic Liquid under Vacuum Condition. *Ionic Liq.: Theory, Prop., New Approaches* **2011**, *2*, 549−564.
(35) Wegner, S.; Janiak, C. Metal Nanoparticles in Ionic Liquids. *Top. Curr. Chem.* **2017**, *375*, 65.
(36) Vanecht, E.; Binnemans, K.; Patskovsky, S.; Meunier, M.; Seo, J. W.; Stappers, L.; Fransaer, J. Stability of Sputter-Deposited Gold Nanoparticles in Imidazolium Ionic Liquids. *Phys. Chem. Chem. Phys.* **2012**, *14*, 5662−5671.

DOI: 10.1021/acs.jpcc.8b06987
J. Phys. Chem. C XXXX, XXX, XXX−XXX